Published in final edited form as:
Med Image Anal. 2008 April ; 12(2): 120–135. doi:10.1016/j.media.2007.08.002.

Inter-subject comparison of MRI knee cartilage thickness

Julio Carballido-Gamio[*], **Jan S. Bauer**, **Robert Stahl**, **Keh-Yang Lee**, **Stefanie Krause**, **Thomas M. Link**, and **Sharmila Majumdar**
MQIR, Department of Radiology, University of California, QB3 Building, 2nd Floor, 201, 1700 – 4th Street, San Francisco, CA 94158, USA

Abstract

In this paper, we present the development and application of current image processing techniques to perform MRI inter-subject comparison of knee cartilage thickness based on the registration of bone structures. Each point in the bone surface which is part of the bone–cartilage interface is assigned a cartilage thickness value. Cartilage and corresponding bone structures are segmented and their shapes interpolated to create isotropic voxels. Cartilage thicknesses are computed for each point in the bone–cartilage interfaces and transferred to the bone surfaces. Corresponding anatomic points are then computed for bone surfaces based on shape matching using 3D shape descriptors called shape contexts to register bones with affine and elastic transformations, and then perform a point to point comparison of cartilage thickness values. An alternative technique for cartilage shape interpolation using a morphing technique is also presented. The cartilage segmentation and morphing were validated visually, based on volumetric measurements of porcine knee images which cartilage volumes were measured using a water displacement method, and based on digital thickness values computed with an established technique. Shape matching using 3D shape contexts was validated visually and against manual shape matching performed by a radiologist. The reproducibility of intra- and inter-subject cartilage thickness comparisons was established, as well as the feasibility of using the proposed technique to build a mean femoral shape, cartilage thickness map, and cartilage coverage map. Results showed that the proposed technique is robust, accurate, and reproducible to perform point to point inter-subject comparison of knee cartilage thickness values.

Keywords

Magnetic resonance imaging (MRI); Cartilage; Segmentation; Shape-based interpolation; Thickness; Shape matching; Shape contexts; Registration

1. Introduction

Osteoarthritis (OA) of the knee is a chronic disease associated with deterioration of the joint cartilage. As OA progresses, the cartilage gets thinner and in severe cases breaks down losing its entire functionality. This pattern is visualized on radiographs as a narrowing of the joint space between the bones and is usually associated with symptoms such as pain, swelling, and decreased motion. However, cartilage morphology cannot be directly assessed on radiographs, which is probably the most important reason why magnetic resonance imaging (MRI) has emerged as the imaging technique of choice for characterization of knee articular cartilage morphology. MRI provides high contrast and high-spatial resolution images to visualize and quantify cartilage degeneration (Peterfy et al., 1994).

*Corresponding author. Tel.: +1 415 514 9665; fax: +1 415 514 9656. Julio.Carballido@radiology.ucsf.edu (J. Carballido-Gamio).

Proper assessment of cartilage morphology with MRI to monitor the progression of joint diseases or related treatments is important. However, cartilage quantification and analysis is not straightforward if true three-dimensional (3D) assessments are desired. The complications increase when we want to compare the knee cartilage of the same patient at different time points or when we want to compare specific joint regions between different patients at any time. These difficulties are the result of anatomical differences, different positioning of patients in the MR scanners, movement of patients during the scans, MR distortions, and other factors. However, there is an increasing interest in performing a compartmental analysis of cartilage morphology and MR relaxometry, and compare the results across different subjects. Typical knee femoral cartilage compartments include for example medial, lateral, and trochlea, and most of the studies perform this comparison by manual determination of the limits of the compartments. The anatomical diagram and MR image of the knee joint in Fig. 1 illustrate the main anatomic components of the knee articulation for the purposes of this paper. The rationale behind the compartmental analysis is that the natural loading conditions of the knee joint due to the biomechanics of the knee articulation are affected by OA leading to non-uniform cartilage degeneration across the articulation. To properly overcome the subjectivity and difficulties of doing an inter-subject compartmental comparison of cartilage knee properties, which increases as the size of the compartments decrease, and to have a better understanding of knee OA, accurate and robust image processing techniques are required. The purpose of this paper is to present image processing techniques to perform inter-subject comparison of knee cartilage thickness in 3D. After MR image acquisition has been performed, cartilage and bone structures of the subjects to be compared are segmented and interpolated based on shape to create isotropic voxels, cartilage thicknesses are computed and transferred to the bone surfaces, shape matching is performed on the bone surfaces, and affine and elastic registrations are applied to perform point to point inter-subject cartilage thickness comparisons.

Semi-automatic approaches to segment cartilage of the knee from MR images obtained with 3D spoiled gradient recalled (SPGR) fat suppressed pulse sequences have been published (Cohen et al., 1999; Stammberger et al., 1999b; Warfield et al., 2000). Because these images offer good contrast at the bone–cartilage interface (bone = dark, cartilage = bright), therefore, the majority of these methods have been based on edge-detection. Recently an automatic approach to segment knee cartilage from images of low field magnets has been reported based on voxel classification (Folkesson et al., 2007), however, the performance of this technique with anatomic images of high field magnets that better depict the knee cartilage morphology and with sequences that offer a different type of contrast than the reported images needs yet to be established. Segmentation of high-spatial resolution images of the knee cartilage is still time consuming and the amount of human interaction is considerable as the result of noise and artifacts encountered in MR images of OA patients. With the aim of reducing the time and effort of manual segmentation while preserving accuracy, a semi-automatic interactive segmentation technique based on edge-detection and Bezier spline interpolation was therefore developed.

Because the through-plane spatial resolution is commonly inferior to the in-plane spatial resolution in MR acquisitions of the knee due to a trade-off between signal to noise ratio and spatial resolution in MRI, proper interpolation has to be performed prior to 3D analysis of the segmented cartilage. Gray-level and shape-based interpolation are the two main interpolation categories and different papers have been published to approach this common problem in image analysis and display (Bors et al., 2002; Chatzis and Pitas, 2000; Grevera and Udupa, 1996; Guo et al., 1995; Herman et al., 1992; Lee and Wang, 2000; Lee and Lin, 2002; Levin, 1986; Migeon et al., 1998a,b; Raya and Udupa, 1990). The technique most widely used for cartilage interpolation is based on distance fields (DFs), can handle branching, and its robustness has been demonstrated (Stammberger et al., 1999a). In this paper we also present an alternative technique to perform cartilage shape-based interpolation, which is a method based on DFs and

elastic registration (warping), and it is known as morphing (Beier and Neely, 1992; Cohen-Or et al., 1998; Lee and Lin, 2002). Morphing techniques are better to handle situations of objects with invaginations (Lee and Lin, 2002) such as those that can occur with focal cartilage lesions. A comparison of both methodologies is also presented.

The morphological cartilage analysis consisted in the computation of its thickness. Different techniques have been proposed in the literature to perform brain cortical thickness (Fischl and Dale, 2000; Haidar and Soul, 2006) and cartilage thickness measurements (Losch et al., 1997; Stammberger et al., 1999a, 2000). The technique used in this work was based on minimum 3D Euclidean distances and has been previously validated for knee cartilage (Stammberger et al., 1999a). This technique suits well with our purposes since cartilage thicknesses can be represented as a sheet, which in this case corresponds to the bone–cartilage interface.

In follow-up studies where MR images of the knee of the same subject are obtained at different time points, image registration is necessary for comparisons of corresponding cartilage regions. Different intra-subject registration techniques have been proposed for this purpose (Kauffmann et al., 2003; Kshirsagar et al., 1998; Lynch et al., 2001; Stammberger et al., 2000). However, it would also be important to create a reference knee and normalize all other knees to this common framework so comparisons of different cartilage properties such as thickness, MR T_2 or MR $T_{1\rho}$ relaxation times could be performed for different populations in the search of a valid biomarker for OA. Since these comparisons involve different subjects, inter-subject registration should be addressed. Few publications have approached the inter-subject registration problem for comparisons of knee cartilage (Carballido-Gamio et al., 2005b; Dardzinski et al., 2002; Slavinsky et al., 2003; Williams et al., 2003). Dardzinski et al. (2002) proposed a 2D technique for inter-subject comparison of MR T_2 relaxation times. Slavinsky et al. (2003) proposed a 3D affine transformation which was followed by a set of 2D elastic registrations using manually identified landmarks to compare maps of cartilage thicknesses. Williams et al. (2003) used a bone statistical shape model to obtain corresponding regions of knee articular cartilage also to compare knee cartilage thicknesses. In this work, semi-automatic affine (intra-subject) and elastic (inter-subject) image registration techniques are proposed, where the cartilage thickness comparisons are based on the registration of the corresponding bone structures (e.g. femoral cartilage comparison based on registration of femora) instead of using the cartilage surfaces themselves, giving robustness to the technique. This is important for OA patients where cartilage shapes can drastically change between subjects. This registration allows point to point comparisons of cartilage characteristics, and it is semi-automatic since the steps involving segmentation require interaction.

Registration is performed based on corresponding anatomic points. In this paper we are presenting 3D shape contexts as shape descriptors that automatically compute such correspondence based on shape matching (Belongie et al., 2002; Carballido-Gamio et al., 2005a,b; Frome et al., 2004). The corresponding anatomic points are used to find the solution to the absolute orientation problem given in Horn et al. (1988) to compute an affine transformation, and also to compute an elastic transformation based on Wenland's radial basis functions (RBFs) with compact support (Fornefett et al., 2001; Wendland, 1995). This is an extension and improvement of our initial work in this field presented at international conferences (a,Carballido-Gamio et al., 2005b).

The structure of this manuscript is as follows: in Section 2, we give a brief technical background related to shape contexts and the corresponding affine and elastic registration techniques used in this work. Section 3, Materials and methods, describes in detail the cartilage segmentation and shape-based interpolation techniques, the computation of cartilage thicknesses and volumes, the application of 3D shape contexts to compute corresponding anatomic points to

perform landmark-based registration of bone structures, the generation of difference cartilage thickness maps, and how a mean bone shape, cartilage thickness and cartilage coverage map were constructed. Qualitative and quantitative validation and results are then shown in Section 4, followed by our discussion and conclusion in Sections 5 and 6, respectively.

2. Background

2.1. Shape contexts

Finding corresponding anatomic points between two structures is a common problem in medical image processing such as registration. Different approaches have been taken to solve this problem and shape descriptors such as those described by Dr. Shen's work (Shen et al., 2001; Shen and Davatzikos, 2002) are excellent examples. Belongie et al. (2002) developed shape descriptors called shape contexts and demonstrated their potential in the field of digit recognition, so Carballido-Gamio et al. (2005a,b) extended Belongie's idea to 3D and presented and validated 3D shape contexts applied to medical image registration.

Point matching is based on 3D shape descriptors that characterize the shape of each point based on histograms of the distribution of points around them. Corresponding points on similar shapes will have similar shape contexts. In comparison to other point matching techniques, shape contexts do not require an equal number of points for the shapes to be compared or segments with specific geometrical configurations. Three-dimensional shape contexts are histograms computed in 3D log-polar spaces on points defining the shape surface, are translation invariant, and can be scaling and rotation invariant under proper normalizations. Fig. 2 shows a representative example of the bin distribution of a 3D shape context where the radial lines of the log-polar histogram binning structure have been avoided for clarity of representation except for those of the two bins highlighted in red. Since the binning structure is log-polar, local as well as global shape information is embedded in the histogram.

In order to find for point p_S in the source shape S the best matching point p_T in the target shape T, points in the surfaces of S and T are sampled and 3D shape contexts are computed for each sampled point to then be compared to each other. Belongie et al. (2002) suggested the χ^2 test statistic (1) as a suitable technique to compare shape contexts since they are histograms of points:

$$\chi^2(h_i, h_j) = \frac{1}{2}\sum_{v=1}^{V}\frac{(h_i(v) - h_j(v))^2}{h_i(v)+h_j(v)}. \quad (1)$$

Here V is the total number of bins in the shape contexts, $h_i(v)$ ($h_j(v)$) the number of points inside the vth bin of the ith (jth) shape context, and $\chi^2(h_i,h_j)$ the cost of matching points p_i and p_j of shapes S and T, respectively.

Given a cost matrix C with entries $c_{i,j} = \chi^2(h_i,h_j)$ a permutation $\pi(i)$ which gives a one-to-one point matching that minimizes the total cost is required. A well known algorithm that satisfies this criterion is the Hungarian method. However, the optimal point matching in this work was a MAT-LAB (The Mathworks, Inc. Natick, MA) implementation of the robust contour matching technique via the order preserving assignment problem or COPAP (Scott and Nowak, 2006). This technique allows the matching of only a fraction of points to increase robustness with respect to shape irregularity and avoids the crossing of landmarks which is physically implausible.

2.2. Affine registration

The affine transformations in this paper were accomplished by using the closed form solution proposed by Horn et al. (1988). Given a set of landmark pairs between two shapes, Horn et al. (1988) find the rotation, translation, and scale factor that will map the source set of landmarks onto the target set so as to minimize the sum of squared distances between them. The solution to the problem of aligning two point sets is formulated in the classic least-squares sense. The residual error between a target landmark and its corresponding transformed source landmark is given by (2)

$$e_i = l_{\mathrm{T},i} - sR(l_{\mathrm{S},i}) - r_0, \tag{2}$$

where s is the scale factor, R the rotation matrix, r_0 the translation, and $l_{\mathrm{S},i}$ and $l_{\mathrm{T},i}$ the corresponding ith source and target landmarks. The problem is then to minimize:

$$\sum_{i}^{N} \|e_i\|^2, \tag{3}$$

where N is total number of landmarks.

By leveraging the centroids of the landmark sets, the translation and scale factor are calculated, while the optimal rotation is computed based on eigenvalue decomposition. Note that while the solution presented above uses orthonormal matrices to represent rotation, a more elegant solution using quaternions is given in Horn (1987).

2.3. Elastic registration

Elastic registration for shape-based interpolation with the morphing technique and inter-subject registration of bone structures was accomplished by using Wendland's RBFs as proposed by Fornefett et al. (2001), which exactly map one landmark set onto the other. These RBFs are compactly-supported and take the following form:

$$\psi_{d,k}(r) = \int_r^\infty (1-t)_+^{\lfloor d/2 \rfloor + k + 1}(t)\mathrm{d}t. \tag{4}$$

Here, d refers to the dimension of space on which ψ is proven to be positive definite, and k designates the function's smoothness C^{2k}. The $(\cdot)_+$ notation encodes the function's limited support as

$$(1-t)_+^x = \begin{cases} (1-t)^x, & 0 \le t < 1, \\ 0, & \text{else.} \end{cases} \tag{5}$$

The mathematical properties also hold for different spatial supports a beyond unity:

$$\psi_a(r) = \psi\left(\frac{r}{a}\right). \tag{6}$$

For a specified space dimension $d > 0$ and smoothness parameter $k \geq 0$ there exists a unique Wendland function $\psi_{d,k}(r) \in C^{2k}(\mathbb{R})$ which is positive definite on $\mathbb{R}_d$ and has a polynomial of

minimal degree *floor(d/2)* + 3*k* + 1, where *floor*(*x*) returns the largest integer ≤*x*. In this paper, the selected function was

$$\psi_{3,1}(r)=(1-r)_{+}^{4}(4r+1). \tag{7}$$

The selection was based on Fornefett et al. (2001) where they chose the pair (*d*,*k*) = (3, 1) as it gave the smallest degree polynomial that was still smooth and differentiable when evaluated at *r* = 0. The scalar input to these functions, *r*, is the distance from a point to a particular source landmark. For (6), Fornefett et al. (2001) suggested a minimum value of *a* equal to 2.98 the maximum landmark displacement for 2D, and 3.66 the maximum landmark displacement for 3D.

3. Materials and methods

After MR images of the knee articulation are acquired, cartilages and corresponding bone structures are segmented and interpolated based on shape to create isotropic voxels. For each point in the bone surfaces corresponding to the bone–cartilage interfaces a thickness value is computed, and for a subset of points in the bone surfaces, 3D shape contexts are calculated to perform shape matching and localized inter-subject comparisons of cartilage thicknesses.

In the following subsections, we describe the details of the image processing steps just mentioned above. Although we focus our application to inter-subject femoral cartilage analysis, the patellar and tibial implementations are straightforward.

3.1. Magnetic resonance imaging

Sagittal MR images of 16 fresh porcine knees were obtained at 3 T (General Electric Healthcare, Milwaukee, WI, USA) using a quadrature knee coil for signal reception. The porcine knees were stored at −80 °C between the measurements, and thawed to room temperature in a water quench for imaging. Images were acquired with a 3D water excitation spoiled gradient echo sequence (WE), in-plane resolution of 0.195 mm × 0.195 mm, and slice thickness of 1.5 mm after reconstruction (Bauer et al., 2006).

In vivo sagittal MR images of five human knees of healthy subjects were also acquired at 3 T (General Electric, Milwaukee, WI) using a GE 8 channel transmit/receive phase-array knee coil. Subjects were positioned supine in the scanner and images were acquired using a 3D SPGR sequence with fat suppression and parallel imaging (ASSET) with acceleration factor of 2, in-plane resolution of 0.312 mm × 0.312 mm, and slice thickness of 1 mm after reconstruction. Each subject was imaged twice in a period of less than 2 weeks for reproducibility purposes.

3.2. Cartilage and bone segmentation

Cartilage was segmented from MR images using a semiautomatic segmentation technique based on Bezier splines and edge-detection. The user placed control points inside the cartilage (e.g. femoral cartilage) following its shape to create a Bezier spline as is shown in Fig. 3a.

In order to find the bone–cartilage interface, edges were enhanced by using anisotropic diffusion filtering (Perona et al., 1994) ($\lambda = 0.25$, number of iterations = 13, $K = 95$), and contrast was improved by using a power law transformation technique (Gonzalez and Woods, 2002) ($c = 1$, $\gamma = 1/3$). Then rays perpendicular to the splines on the control points were traced towards the bone–cartilage interface to a distance equal to a width of approximately 15 pixels. From these positions, line profiles were computed back to the cartilage using bicubic interpolation

with an average of two points per pixel (Fig. 3b) for a total of 30 points. After computing the first derivative of brightness of the line profiles, the maximum values were taken as the bone–cartilage interface for each control point.

The original image was taken again, edges were enhanced with anisotropic diffusion filtering ($\lambda = 0.25$, number of iterations = 7, $K = 50$), and contrast was improved by a power law transformation ($c = 1$, $\gamma = 2$) to find the articular surface. New line profiles were computed in opposite direction of those shown in Fig. 3b as is shown in Fig. 3c, and based on the maxima of the first derivatives of brightness positions for the articular surface were found. The first and last points of the splines remained in their original positions at all times.

Since edges are not always well defined at the patello-femoral and tibio-femoral articulations, an automatic thickness correction algorithm was implemented in the segmentation process. The mean value plus one fourth of the standard deviation of the distances between corresponding points for the found bone–cartilage and articular surfaces was computed. For the pairs of points above this thickness value, a new articular edge was searched since there was a higher confidence on the identified bone–cartilage edges. For this thickness correction step, the original image was taken again and filtered with anisotropic diffusion ($\lambda = 0.25$, number of iterations = 1, $K = 5$). No contrast enhancement was applied this time. The new articular edges were computed as the last peaks of the first derivative of brightness of the new line profiles. If no local maxima were found, the control points were not moved from the initial computed edges. The user had the opportunity of manually adjusting the position of any control point at any time. Based on the found edges, new Bezier splines were created to represent the bone–cartilage interface and the articular surface, giving also an automatic labeling as is shown in Fig. 3d with color coding (cyan = bone–cartilage interface; magenta = articular surface). The labeling of surfaces as bone–cartilage and articular was essential for our cartilage thickness computation.

The technique allows performing segmentation of disconnected cartilage as can happen with subjects with advanced OA by positioning a Bezier spline inside of each cartilage component. In order to segment a contiguous slice, only the corresponding end points for each Bezier spline were needed doing the segmentation based on information from the closest segmented slice.

Bone structures were segmented with a similar technique as that used for the bone–cartilage interface. In fact, the section of the bone surface corresponding to the bone–cartilage interface was taken from the cartilage segmentation. Fig. 4 shows the corresponding femoral bone segmentation of the images shown in Fig. 3.

3.3. Shape-based interpolation of segmented cartilage and bone

After cartilage and bone structures were segmented using the semi-automatic technique described in the previous section, the contours were used to interpolate its shape to create isotropic voxels with a side length equal to the in-plane resolution (squared pixels after reconstruction). This interpolation was done with a technique based on DFs which was previously validated for cartilage (Stammberger et al., 1999a).

For each slice, the Bezier splines representing the bone–cartilage interfaces and articular surfaces were evaluated and discretized. For each contour (C_m) representing a cartilage segment in a slice z a bounding box was computed followed by its DF_m (Breu et al., 1995), where the value of each pixel q was computed by using (8):

$$DF_m(q) = \begin{cases} -dist(q, C_m), & \text{if } q \in C_m, \\ dist(q, C_m), & \text{otherwise}, \end{cases} \tag{8}$$

where $dist(\cdot)$ is the Euclidean distance function. Then DFs were put together with a minimum function in case of overlapping of bounding boxes, and a new global bounding box was created for further processing.

New DFs between slices were created by using linear interpolation:

$$DF_t=(1-t)DF_S+tDF_T, \tag{9}$$

where DF_S, DF_T, and DF_t, represent the DF of the *source*, *target*, and *source* + *t* slices, respectively; and *t* is a variable that can take values in the range of [0, 1]. Then the interpolated shape was extracted from the interpolated DF_t by using (10):

$$cart_t=\{q|DF_t(q)\leq 0\}, \tag{10}$$

where $cart_t$ represents the set of pixels *q* inside or in the border of the interpolated cartilage at slice *source* + *t*.

Shape-based interpolation of bone structures was accomplished by applying the same technique to the bone contours.

An alternative cartilage shape-based interpolation technique using morphing was also developed. For this purpose the splines representing the cartilage contours were evaluated and discretized, and DFs were computed as previously described in this section.

From the pair of contiguous segmented slices under evaluation, the slice with more disconnected cartilage segments was selected, and each contour was matched to a cartilage segment on the other slice based on minimum Euclidean distances. Based on the relative positions to the spline end points, an artificial matching of approximately 20 points was done to obtain corresponding landmarks for the source and target slices.

The positions of landmarks at slice *source* + *t* were computed with linear interpolation, and then by using RBFs with compact support (Fornefett et al., 2001; Wendland, 1995), the warping parameters were computed to elastically register them to the source and target landmarks. The computed registration parameters were then applied to the coordinates of the slice *source* + *t*, and by using bilinear interpolation two new distance fields were obtained: DF'_S and DF'_T. The interpolated distance field DF_t was computed by linear interpolation of the new DFs', and the pixels representing the interpolated cartilage shape were obtained by using (10).

3.4. Cartilage thickness and volume

Labeling of the cartilage surfaces as bone–cartilage interface and articular surface is required for the computation of 3D cartilage thickness measurements using either 3D minimum Euclidean distances or a normal vector approach. Unfortunately, this information was lost for the interpolated cartilage in the two shape-based interpolation techniques described in the previous section, and an automatic labeling technique had to be developed. This labeling was based on the end points of the cartilage segments and Euclidean distances between them.

For each point on the bone–cartilage surface, the closest point on the articular surface was found and the corresponding distance was assigned as its thickness value. So each point in the bone surface corresponding to the bone–cartilage interface had a thickness value assigned to it. For validation purposes, this process was done for three different cases for the porcine knees: (1) cartilage with no shape interpolation (anisotropic resolution); (2) cartilage with shape interpolation using only DFs; and (3) cartilage with shape interpolation using the morphing

approach. Cartilage volume was also digitally computed for these three cases for the porcine knees, and it was done by counting the number of cartilage voxels.

Although an indirect approach to validate the accuracy of the segmentation and shape interpolation techniques, the femoral cartilage of all porcine knees was scraped off after image acquisition and their volume was measured using a water displacement method, which was then compared to the digital values.

The in vivo precision of the segmentation and shape-based interpolation techniques was assessed by computing the coefficient of variation (CV) based on previously reported techniques to measure the short-term precision of a technique (Glüer et al., 1995). Human cartilage thicknesses of the five pairs of baseline and follow-up acquisitions were used for this purpose.

3.5. Registration

Corresponding anatomic points between femora were computed by using 3D shape contexts (Carballido-Gamio et al., 2005b) and COPAP (Scott and Nowak, 2006). Shape-interpolated voxels representing the source and target bone shapes were uniformly sampled in space (approximately every 67 voxels for shapes with approximately 135,000 surface points). Since shape contexts are not rotation invariant, Belongie et al. (2002) proposed to find the tangent vector at each point and use it as the positive x-axis to compute 2D rotation invariant shape contexts. Frome et al. (2004) accomplished 3D rotation invariance by computing 3D normal vectors to the shapes and aligning the positive z-axis of 3D shape contexts to them, followed by a series of rotations around this axis to remove the left degree of freedom. Since the final goal of Carballido-Gamio et al. (2005a) was image registration, 3D rotational effects of medical images were reduced by a previous 3D alignment of source and target shapes based on the 3D registration of their middle slices assuming similar shapes, orientations, and fields of view. In this work, initial 3D alignment was accomplished by using the iterative closest point (ICP) algorithm (Besl and McKay, 1992).

For each point in the sampled surface, a 3D shape context representing the point distribution of the relative remaining points was computed. The histogram bins were uniform in a 3D log-polar space: r [1/8, r_{max}], θ [0,2π) and φ [0,π]. Eleven values for r, 11 values for θ, and 6 values for φ were used in this paper for a total of 726 bins. Shape contexts were made scaling invariant by normalizing the radial distances by the mean distance of all the pair-wise distances of the points representing the shape (Belongie et al., 2002). The value of r_{max} was equal to the maximum distance between two surface points.

A total of 30 shape contexts were uniformly selected from the target shape and approximately 75% of them were matched to the source by using COPAP (Scott and Nowak, 2006). Based on the computed corresponding anatomic points and by using the closed form solution given by Horn et al. (1988), an affine transformation was obtained and applied to the source shape. When the target and source bones correspond to the same subject, the application of this affine transformation allows intra-subject point to point comparisons of cartilage properties such as thickness.

For the elastic registration after the affine transformations (i.e. for inter-subject comparisons), a new set of 200 target shape contexts were uniformly selected and approximately 75% of them were matched to the source shape by using COPAP. Based on the computed corresponding anatomic points, elastic registration parameters were calculated (Fornefett et al., 2001) and applied to the source shape.

In order to compare point to point the source and target bone–cartilage interfaces after registration, their points were matched based on minimum Euclidean distances, and maps representing their thickness differences were computed.

It is important to clarify that the cartilage thicknesses were calculated prior to the registrations, so their values remained unchanged during the transformations.

In order to validate the accuracy of the shape matching proposed in this paper based on 3D shape contexts and COPAP, a radiologist selected seven pairs of corresponding anatomic points on the baseline and follow-up scans for each subject. Based on these manual anatomical correspondences 5 intra-subject and 8 inter-subject affine transformations were computed. These 13 transformations were also computed in two additional ways for validation purposes. First, the target anatomic points were those selected by the radiologist, and the corresponding source anatomic points were computed automatically based on shape matching. Second, both the target and source anatomic corresponding points were computed automatically as previously described in this section. Final Euclidean distances between target and source corresponding anatomic points were computed for the three different cases and compared. Average minimum Euclidean distances between bone surfaces after registration were also evaluated.

To further validate our technique, a precision study was implemented where 5 intra- and 10 inter-subject localized cartilage thickness analyses were computed twice to asses a CV by using previously reported techniques (Glüer et al., 1995).

The feasibility of implementing a comparison of a small predefined region of interest between different subjects was also established as well as its reproducibility.

3.6. Mean shape, cartilage thickness and coverage map

A mean femoral shape was constructed based on previously reported techniques (Cootes and Taylor, 2004) and using 3D shape contexts with COPAP to identify corresponding anatomic points across the population. Basically all femoral bones are translated so their centers of gravity are at the origin. One sample is selected as an initial estimate of the mean shape and scaled so that $|\vec{x}| = 1$, where $\vec{x}$ is a vector with the coordinates of the mean shape. This first estimate is recorded as $\overline{x_0}$ to define a reference frame. Then all shapes are aligned with the current estimate of the mean shape, and the mean shape is re-estimated based on the aligned shapes. This is an iterative process where each time there are constraints that are applied to the current estimate of the mean by aligning it with $\overline{x_0}$ and scaling so that $|\vec{x}| = 1$. The process is terminated when there are no substantial changes of the mean shape after an iteration. During this alignment process the inter-subject comparisons of knee cartilage thicknesses were performed and recorded to create a mean femoral cartilage thickness map. Because the area on the bone surface that is covered by cartilage changes from subject to subject, a cartilage map representing the probability of bone being covered by cartilage was also constructed.

To further validate the feasibility of using a mean femoral shape and mean cartilage thickness map as a fixed reference instead of performing one-to-one inter-subject comparisons, one subject with severe OA was scanned at a different field strength (1.5 T) and spatial resolution (0.235 mm × 0.235 mm × 2 mm), and his femoral cartilage was compared to the model. Same segmentation and shape-interpolation techniques were used as well as registration strategies, however, the final isotropic spatial resolution was of 0.235 mm.

4. Results

4.1. Cartilage segmentation and shape interpolation

A Pearson correlation coefficient $r = 0.83$ ($p < 0.001$) was found for the cartilage volume of 16 porcine knees measured with the water displacement method, and the digitally computed volume obtained from interpolated cartilage with DFs, interpolated cartilage with morphing, and no interpolated cartilage.

Digital volumetric results were also compared to the water displacement technique by using the Bland–Altman method, which is a robust technique that quantifies the strength of agreement between two methods of measurement (rather than the relationship between them) by comparing the difference in measurements for each subject. Digital volumetric measurements showed good agreement with the water displacement results since all volumetric differences were inside of the band of 2 standard deviations of the difference of the measurements. The Bland–Altman analysis basically demonstrated that the digital volumetric techniques were as good as the water displacement method.

Cartilage thickness analysis revealed a Pearson correlation value $r = 0.95$ ($p < 0.001$) for the measurements based on the shape-interpolated cartilage with DFs (most common technique) and the morphed cartilage. Both thickness measurements showed good agreement according to the Bland–Altman method. Examples of 3D cartilage thickness maps of human knees for different shape-interpolation strategies are shown in Fig. 5.

The reproducibility of the intra-subject cartilage thickness measurements is reported in Table 1 for the femoral medial, trochlear, and lateral compartments, as well as for the whole femoral cartilage using DFs as well as morphing for shape interpolation. For the baseline and follow-up scans the femoral cartilage compartments were manually delineated and their mean cartilage thickness values were used to generate a CV.

4.2. Shape matching

The performance of 3D shape contexts for matching of corresponding anatomic points was validated visually and quantitatively. Table 2 summarizes the quantitative intra-subject shape matching validation. In this table, mean distances of corresponding anatomic points as well as femoral surface errors are shown for different scenarios. Since the true femoral anatomical correspondences were unknown, we computed the surface errors as defined in Gefen et al. (2003), where surface error is defined as the average Euclidean distance, where the distance is measured between a point on the surface of a test shape's structure and the closest point to it on the corresponding reference shape's structure. The numbers presented in Table 2 are the results of intra-subject follow-up to baseline registrations.

Similar to Table 2, quantitative results for the inter-subject validation are shown in Table 3. In order to generate this table, one subject was selected as the target for both the baseline and follow-up scans, and all other subjects were matched to it yielding a total of 8 registrations (4 baselines and 4 follow-ups).

Visual validation was implemented in different ways based on renderings of the bone structures and anatomic points. The position of automatically computed source anatomic points based on the manually selected target anatomic points given by a radiologist was observed as is shown in Fig. 6. Similar visual validation was implemented for the automatically computed target and source anatomic points as is shown in Fig. 7.

4.3. Cartilage thickness comparisons

Figs. 8 and 9 show examples of the results of localized cartilage thickness comparisons based on elastic femoral bone registrations, demonstrating the feasibility of the technique. In these figures it is evident that corresponding anatomic locations are being compared between the source and target maps. In the difference thickness maps, blue areas represent source thicker cartilage points, while red areas represent thinner points. Although the difference thickness maps can be displayed in the warped coordinates, Figs. 8 and 9 display them in the original source coordinates. This is possible because the cartilage thickness maps were calculated before any registration and each point in the bone–cartilage interfaces had a thickness value assigned to it.

In terms of the precision of the localized intra-subject comparisons of cartilage thicknesses, Table 4 summarizes the results, while Tables 5 and 6 summarize all the inter-subject longitudinal comparisons. The localized intra-subject reproducibility reported in Table 4 is based on five subjects. For this purpose, the baseline femoral cartilage compartments were manually delineated while those of the follow-up scans were automatically selected. Point matching was then performed between corresponding compartments based on the target cartilage, and the mean cartilage thickness values of the matched baseline and follow-up points were used to generate a CV.

For comparison purposes, the precision of performing inter-subject comparisons of mean cartilage thickness values with manual delineation of cartilage compartments was also assessed and Table 5 shows the corresponding results for 10 cases.

Table 6 shows the precision results for the femoral inter-subject localized cartilage thickness comparisons for 10 cases. Target cartilage compartments were manually delineated while those of the source were automatically computed. For each point in the bone–cartilage interface at each compartment in the target subject, one point in the corresponding compartment in the source bone–cartilage interface was assigned and their cartilage thickness differences computed. The values of these differences at each compartment were used to generate a CV.

Basically, Tables 5 and 6 show two different ways of comparing cartilage thickness values between two subjects: (1) difference of the mean cartilage thicknesses with no registration; and (2) mean values of point difference thicknesses as those shown in Figs. 8 and 9.

The feasibility results of comparing a predefined small region of interest are shown in Fig. 8. The CV for this scenario based on 4 comparisons was of 6.86%.

4.4. Mean shape, cartilage thickness and coverage map

Results of testing the feasibility to use the proposed technique to build a mean femoral shape, mean femoral cartilage thickness map, as well as a cartilage coverage map are displayed in Figs. 9 and 10. These results were generated based on five subjects. The global mean femoral cartilage thickness was 1.71 mm and 1.91 mm for bone regions with probability of being covered by cartilage of greater than zero and greater than 0.5, respectively (Fig. 10). The mean cartilage thickness for regions always covered by cartilage was 2.09 mm. In the mean femoral cartilage thickness map displayed in Fig. 9, blue regions represent thick cartilage while red regions depict thin cartilage. In the cartilage coverage map showed in Fig. 10, dark and yellow regions represent regions of the bone–cartilage interface with high and low probability of being covered by cartilage, respectively.

Visual results of the point comparisons of the advanced OA subject to the mean cartilage thickness map are displayed in Fig. 9. For this case a mean difference of −0.31 mm was detected with a maximum difference of −2.84 mm.

5. Discussion

Osteoarthritis (OA) is the most common form of arthritis in the world and it is a major cause of morbidity and disability in the US and Europe. It is expected that in 2020, 59.4 million Americans will be affected by some form of osteoarthritis (Boulos et al., 2003).

Different morphological, molecular, and biochemical biomarkers for predicting or evaluating the degree of OA of the knee have been investigated (Gray et al., 2004), including cartilage thickness and volume. These morphological biomarkers have received substantial attention as thinning of cartilage is a common manifestation of this pathology. MRI in contrast to radiographs allows the direct visualization and quantification of cartilage morphology and is therefore the imaging technique of choice.

It is important to quantify knee cartilage morphology to monitor the progression of degenerative joint disease or related treatments, and when this assessment is based on medical images such as MRI, accurate and robust image processing tools are required to perform 3D cartilage quantification and analysis. We have presented and validated a set of techniques to accomplish this goal for intra- and inter-subject scenarios.

The segmentation technique proposed in this paper allows the segmentation of 1 slice in about 30 s with no significant loss of accuracy as it was quantitatively demonstrated with the Bland–Altman method and correlation coefficients based on the cartilage volumetric measurements of the porcine knees.

Volumetric and thickness results could suggest at first glance that there is no need for shape interpolation of cartilage. However, there are certain applications such as analysis and follow-up of focal cartilage lesions where shape interpolation plays a central role. Inspection showed that the quality of the cartilage thickness maps was enhanced by using the morphing technique for shape interpolation demonstrating a smoother transition from slice to slice compared to the DFs approach, which in some occasions introduced small artifacts. This improvement however, also came with a major computational cost to perform the corresponding point matching and warping. If shape-interpolation based only on DFs is desired, then cubic interpolation instead of linear would be a better choice. Both techniques however, demonstrated excellent levels of reproducibility as is shown in Table 1. The reproducibility of 2.5% or better for the intra-subject mean cartilage thickness measurements was comparable to those previously reported in the literature (Glaser et al., 2006;Gray et al., 2004). Further validation with a larger data set of patients with focal lesions is still necessary to demonstrate the advantages of the morphing technique.

In follow-up studies, or studies involving Different patient populations, proper image processing methods are required to compare common regions or points of cartilage. We have presented and validated a semi-automatic registration technique to accomplish this task. The alignment to perform such comparisons is based on the registration of bone structures instead of using the cartilage surfaces themselves, giving robustness to the technique. This is important for OA patients where cartilage shapes can drastically change between subjects. Since the technique requires the shapes of the bones to perform the alignment, it is still dependent on the segmentations. However, 3D shape contexts are robust enough to capture corresponding points on the structures of interest, and robust automatic segmentation techniques are under continuous development. The shape matching technique as it was presented is translation invariant, scaling invariant, and by the initial application of ICP registration its rotational invariance is well handled. This shape matching does not require an equal number of points for the shapes to be compared or segments with high curvature, allows the application of non-linear registration techniques that enable local or global deformations as proposed by Fornefett et al. (2001), and is simple and easy to apply.

Intra-subject shape matching validation indicated that affine transformations based on automatically computed target and source anatomical points yielded similar results than the affine transformations based on the set of corresponding anatomic points manually selected by a radiologist as can be observed in Table 2. The Difference of mean distances between the target and source points selected by the radiologist was smaller then the smallest voxel dimension between the automatic and manual cases after affine registration. This Difference was slightly higher when the source anatomic points were automatically computed based on the target anatomic points given by the radiologist, however, it was still less than the diagonal of the shape-interpolated voxels. The automatic case yielded the smallest surface error.

Inter-subject shape matching validation also indicated that affine transformations based on automatically computed target and source anatomic points yielded similar results than the affine transformations based on the set of corresponding anatomic points manually selected by a radiologist as can be observed in Table 3. The Difference of the mean distances between target and source points selected by the radiologist was slightly larger after affine registration compared to the intra-subject case; however, it was less than two times the diagonal of the shape-interpolated voxels. The automatic inter-subject shape matching yielded the smallest surface error as in the intra-subject case.

Intra-subject reproducibility of mean cartilage thickness measurements based on point matching of manually selected target compartments and automatically delimited source compartments (Table 4) yielded similar results than the mean intra-subject cartilage thickness comparisons based on manual selection of compartments (Table 1). This fact indicates that the whole process is highly reproducible: imaging, segmentation, shape-based interpolation, cartilage thickness measurements, intra-subject femoral alignments, and point matching for localized cartilage thickness comparisons. Visualization of the inter-subject matching as is demonstrated in Figs. 6 and 7 demonstrates that corresponding anatomic points were properly computed.

Successful point to point inter-subject cartilage thickness comparisons were accomplished with a general precision improvement when compared to the manual case as can be observed in Tables 5 and 6. It is important to clarify that for the intra- and inter-subject cases with no registration, the mean cartilage thickness values of the compartments were utilized to calculate the CVs, while for the intra- and inter-subject cases with registration, the mean values and the mean values of the cartilage thickness Differences of matched points were used, respectively. Local reproducibility of other cartilage properties such as cartilage MR T_2 relaxation times have been reported for the intra-subject case (Glaser et al., 2006), but no local inter-subject knee cartilage thickness reproducibility measurements have been published. However, in a recent international conference similar reproducibility results were presented using a Different registration approach (Williams et al., 2006).

Our technique also demonstrated good levels of reproducibility (6.86%) when a small region of interest was predefined in one subject and matched to the other four. Again, inspection of Fig. 8 corroborated our results.

Visual representation of localized cartilage thickness differences in the original coordinates of the source subject as is shown in Figs. 8 and 9 was possible since cartilage thickness measurements were performed before any registration, and each point in the bone–cartilage interface had a thickness value assigned to it. This is important because our goal was only to compare cartilage thicknesses at corresponding anatomic locations, so we wanted to keep the original thickness values from the source and target subjects. If affine and elastic transformations were applied to the source cartilage, and then cartilage thicknesses were computed, the source thickness values would then depend on the target subject, since the

transformation parameters include scaling and non-linear transformations that are the result of shape matching. By keeping the original thickness values, the Difference between healthy an OA subjects can be better appreciated. However, normalization of cartilage thickness values based on the femoral bone geometry as is commonly done for the cartilage volume could be applied.

We have also demonstrated the feasibility of constructing a mean femoral bone shape, cartilage thickness map, and cartilage coverage map, which opens the possibility of many OA potential studies and technical developments. A mean shape could be used to automatically segment bones of the knee articulation which could benefit biomechanical analyses of the knee joint. Different mean shapes and cartilage thickness maps could be used for Different OA population studies, and cartilage coverage maps could be employed to perform automatic cartilage segmentation. A larger data set is obviously needed in order to have a representative model that includes more possible variations of the femoral bone shape and cartilage thickness values. However, the comparison of a subject with severe OA and the initial model constructed in this paper demonstrated that corresponding anatomic regions were compared (Fig. 9), and that as it was expected, the mean of the point-wise Difference of cartilage thicknesses showed that the subject with severe OA had thinner cartilage than the mean femoral cartilage thickness based on healthy volunteers.

Although the technique has been applied for inter-subject comparison of femoral cartilage thickness measurements, it could also be used to compare other important parameters derived from MR images such as T_2 or $T_{1\rho}$ relaxation times. If only comparison of anatomic regions is desired (not point to point), 3D shape contexts could be then employed to establish correspondence of common areas with no necessity of elastic registration, which probably could improved the precision of the technique.

6. Conclusions

It is important to asses the quantification of knee cartilage morphology to monitor the progression of joint diseases or related treatments. When this assessment is based on medical images such as MRI, accurate and robust image processing tools are required. We have presented and validated a set of techniques to accomplish this goal for the intra- and inter-subject analysis.

Acknowledgments

The authors would like to acknowledge Belinda Li from GE Medical Systems for providing the WE sequence, Dr. Jin Zuo for providing the human 3 T knee MRI data set, and J.P. Slavinsky for his seminal work on inter-subject comparison of knee cartilage at our lab. This work was supported by NIH grant RO1 AR46905, RO1 AG17762, and UO1 AR-06-006.

References

Bauer JS, Krause SJ, Ross CJ, Krug R, Carballido-Gamio J, Ozhinsky E, Majumdar S, Link TM. Volumetric cartilage measurements of porcine knee at 1.5-T and 3.0-T MR imaging: evaluation of precision and accuracy. Radiology 2006;241 (2):399–406. [PubMed: 17057067]

Beier T, Neely S. Feature-based image metamorphosis. Comput Graph 1992;26 (2):35–42.

Belongie S, Malik J, Puzicha J. Shape matching and object recognition using shape contexts. IEEE Trans PAMI 2002;24 (4):509–522.

Besl PJ, McKay HD. A method for registration of 3D shapes. IEEE Trans Pattern Anal Mach Intell 1992;14 (2):239–256.

Bors AG, Kechagias L, Pitas I. Binary morphological shape-based interpolation applied to 3D tooth reconstruction. IEEE Trans Med Imaging 2002;21 (2):100–108. [PubMed: 11929098]

Boulos P, Papaioannou A, Beattie K, Adachi JD. Measurement techniques for the detection of early osteoarthritis, business briefing: long-term healthcare strategies. 2003

Breu H, Gil J, Kirkpatrick D, Werman M. Linear time Euclidean distance transform algorithms. IEEE Trans Pattern Anal Mach Intell 1995;17 (5):529–533.

Carballido-Gamio, J.; Lee, K-Y.; Majumdar, S. Automatic 3D point matching of segmented images using shape contexts. ISMRM Proceedings; 2005. 2005

Carballido-Gamio J, Bauer J, Lee KY, Krause S, Majumdar S. Combined image processing techniques for characterization of MRI cartilage of the knee. Conf Proc IEEE Eng Med Biol Soc 2005b;3:3043–3046. [PubMed: 17282885]

Chatzis V, Pitas I. Interpolation of 3D binary images based on morphological skeletonization. IEEE Trans Med Imaging 2000;19 (7):699–710. [PubMed: 11055785]

Cohen ZA, McCarthy DM, Kwak SD, Legrand P, Fogarasi F, Ciaccio EJ, Ateshian GA. Knee cartilage topography, thickness, and contact areas from MRI: in-vitro calibration and in-vivo measurements. Osteoarthritis Cartil 1999;7 (1):95–109.

Cohen-Or D, Levin D, Solomovici A. Three-dimensional distance field metamorphosis. ACM Trans Graph 1998;17 (2):116–141.

Cootes TF, Taylor CJ. Statistical Models of Appearance for Computer Vision. 2004

Dardzinski, BJ.; Schmithorst, VJ.; Mosher, TJ.; Smith, MB. Cartilage warping: a technique for inter-subject comparison of T2 relaxation time. ISMRM Proceedings; 2002. 2002

Fischl B, Dale AM. Measuring the thickness of the human cerebral cortex from magnetic resonance images. Proc Natl Acad Sci USA 2000;97 (20):11050–11055. [PubMed: 10984517]

Folkesson J, Dam EB, Olsen OF, Pettersen PC, Christiansen C. Segmenting articular cartilage automatically using a voxel classification approach. IEEE Trans Med Imaging 2007;26 (1):106–115. [PubMed: 17243589]

Fornefett M, Rohr K, Stiehl HS. Radial basis functions with compact support for elastic registration of medical images. Image Vis Comput 2001;19 (1):87–96.

Frome, A.; Huber, D.; Kolluri, R.; Bullow, T.; Malik, J. Recognizing objects in range data using regional point descriptors. European Conference on Computer Vision Proceedings; 2004. 2004

Gefen S, Tretiak O, Nissanov J. Elastic 3D alignment of rat brain histological images. IEEE Trans Med Imaging 2003;22 (11):1480–1489. [PubMed: 14606681]

Glaser C, Mendlik T, Dinges J, Weber J, Stahl R, Trumm C, Reiser M. Global and regional reproducibility of T2 relaxation time measurements in human patellar cartilage. Magn Reson Med 2006;56 (3):527–534. [PubMed: 16894587]

Glüer CC, Blake G, Blunt BA, Jergas M, Genant HK. Accurate assessment of precision errors: how to measure the reproducibility of bone densitometry techniques. Osteoporosis Int 1995;5:262–270.

Gonzalez, RC.; Woods, RE. Digital Image Processing. Prentice Hall; 2002. Power-law transformations; p. 80-84.

Gray ML, Eckstein F, Peterfy C, Dahlberg L, Kim YJ, Sorensen AG. Toward imaging biomarkers for osteoarthritis. Clin Orthop Relat Res 2004;(427 Suppl):S175–S181. [PubMed: 15480063]

Grevera GJ, Udupa JK. Shape-based interpolation of multidimensional gray-level images. IEEE Trans Med Imaging 1996;15 (6):881–892. [PubMed: 18215967]

Guo JF, Cai YL, Wang YP. Morphology-based interpolation for 3D medical image reconstruction. Comput Med Imaging Graph 1995;19 (3):267–279. [PubMed: 7641171]

Haidar H, Soul JS. Measurement of cortical thickness in 3D brain MRI data: validation of the Laplacian method. J Neuroimaging 2006;16 (2):146–153. [PubMed: 16629737]

Herman GT, Zheng J, Bucholtz CA. Shape-based interpolation. IEEE Comput Graph Appl 1992;12 (3): 69–79.

Horn BKP. Closed form solution of absolute orientation using unit quaternions. J Opt Soc A 1987;4 (4): 629–642.

Horn BKP, Hilden HM, Negahdaripour S. Closed form solution of absolute orientation using orthonormal matrices. J Opt Soc A 1988;5 (7):1127–1135.

Kauffmann C, Gravel P, Godbout B, Gravel A, Beaudoin G, Raynauld JP, Martel-Pelletier J, Pelletier JP, de Guise JA. Computer-aided method for quantification of cartilage thickness and volume changes

using MRI: validation study using a synthetic model. IEEE Trans Biomed Eng 2003;50 (8):978–988. [PubMed: 12892325]

Kshirsagar AA, Watson PJ, Tyler JA, Hall LD. Measurement of localized cartilage volume and thickness of human knee joints by computer analysis of three-dimensional magnetic resonance images. Invest Radiol 1998;33 (5):289–299. [PubMed: 9609488]

Lee TY, Lin CH. Feature-guided shape-based image interpolation. IEEE Trans Med Imaging 2002;21 (12):1479–1489. [PubMed: 12588032]

Lee TY, Wang WH. Morphology-based three-dimensional interpolation. IEEE Trans Med Imaging 2000;19 (7):711–721. [PubMed: 11055786]

Levin D. Multidimensional reconstruction by set-valued approximation. IMA J Numer Anal 1986;6:173–184.

Losch A, Eckstein F, Haubner M, Englmeier KH. A noninvasive technique for 3-dimensional assessment of articular cartilage thickness based on MRI. Part 1: Development of a computational method. Magn Reson Imaging 1997;15 (7):795–804. [PubMed: 9309610]

Lynch, JA.; Zaim, S.; Zhao, J.; Peterfy, CG.; Genant, HK. Automating measurement of subtle changes in articular cartilage from MRI of the knee by combining 3D image registration and segmentation. SPIE, Medical Imaging Proceedings; 2001. 2001

Migeon B, Charreyron R, Deforge P, Langlet A, Renard J, Marche P. An automatic spline-based contour interpolation for the 3D reconstruction of a thin walled elastic tube. J Biomech 1998a;31:70.

Migeon, B.; Charreyron, R.; Deforge, P.; Marche, P. Improvement of morphology-based interpolation. Proceedings; 1998b.

Perona, P.; Shiota, T.; Malik, J. Geometry-Driven Diffusion in Computer Vision. Kluwer Academic Publishers; 1994. Anisotropic diffusion; p. 73-92.

Peterfy CG, van Dijke CF, Janzen DL, Gluer CC, Namba R, Majumdar S, Lang P, Genant HK. Quantification of articular cartilage in the knee with pulsed saturation transfer subtraction and fat-suppressed MR imaging: optimization and validation. Radiology 1994;192 (2):485–491. [PubMed: 8029420]

Raya SP, Udupa JK. Shape-based interpolation of multidimensional objects. IEEE Trans Med Imaging 1990;9 (1):32–42. [PubMed: 18222748]

Scott C, Nowak R. Robust contour matching via the order-preserving assignment problem. IEEE Trans Image Process 2006;15 (7):1831–1838. [PubMed: 16830905]

Shen D, Davatzikos C. HAMMER: hierarchical attribute matching mechanism for elastic registration. IEEE Trans Med Imaging 2002;21 (11):1421–1439. [PubMed: 12575879]

Shen D, Herskovits EH, Davatzikos C. An adaptive-focus statistical shape model for segmentation and shape modeling of 3D brain structures. IEEE Trans Med Imaging 2001;20 (4):257–270. [PubMed: 11370893]

Slavinsky, JP.; Ozhinsky, E.; Majumdar, S. A combination of rigid and elastic registration methods for a standard atlas of the knee. ISMRM Proceedings; 2003. 2003

Stammberger T, Eckstein F, Englmeier KH, Reiser M. Determination of 3D cartilage thickness data from MR imaging: computational method and reproducibility in the living. Magn Reson Med 1999a;41 (3):529–536. [PubMed: 10204876]

Stammberger T, Eckstein F, Michaelis M, Englmeier KH, Reiser M. Interobserver reproducibility of quantitative cartilage measurements: comparison of B-spline snakes and manual segmentation. Magn Reson Imaging 1999b;17 (7):1033–1042. [PubMed: 10463654]

Stammberger T, Hohe J, Englmeier KH, Reiser M, Eckstein F. Elastic registration of 3D cartilage surfaces from MR image data for detecting local changes in cartilage thickness. Magn Reson Med 2000;44 (4):592–601. [PubMed: 11025515]

Warfield SK, Kaus M, Jolesz FA, Kikinis R. Adaptive, template moderated, spatially varying statistical classification. Med Image Anal 2000;4 (1):43–55. [PubMed: 10972320]

Wendland H. Piecewise polynomial, positive definite and compactly supported radial basis functions of minimal degree. Adv Comput Math 1995;4:389–396.

Williams, TG.; Taylor, CJ.; Gao, Z-X.; Waterton, JC. Corresponding locations of knee articular cartilage thickness measurements by modelling the underlying bone. MIUA Proceedings; 2003. 2003

Williams, TG.; Holmes, AP.; Maciewicz, RA.; Waterton, JC.; Nash, AF.; Taylor, CJ. Improved repeatability of cartilage thickness measurements from MRI using anatomically corresponding regions of interest. OARSI 2006 Proceedings; 2006. 2006

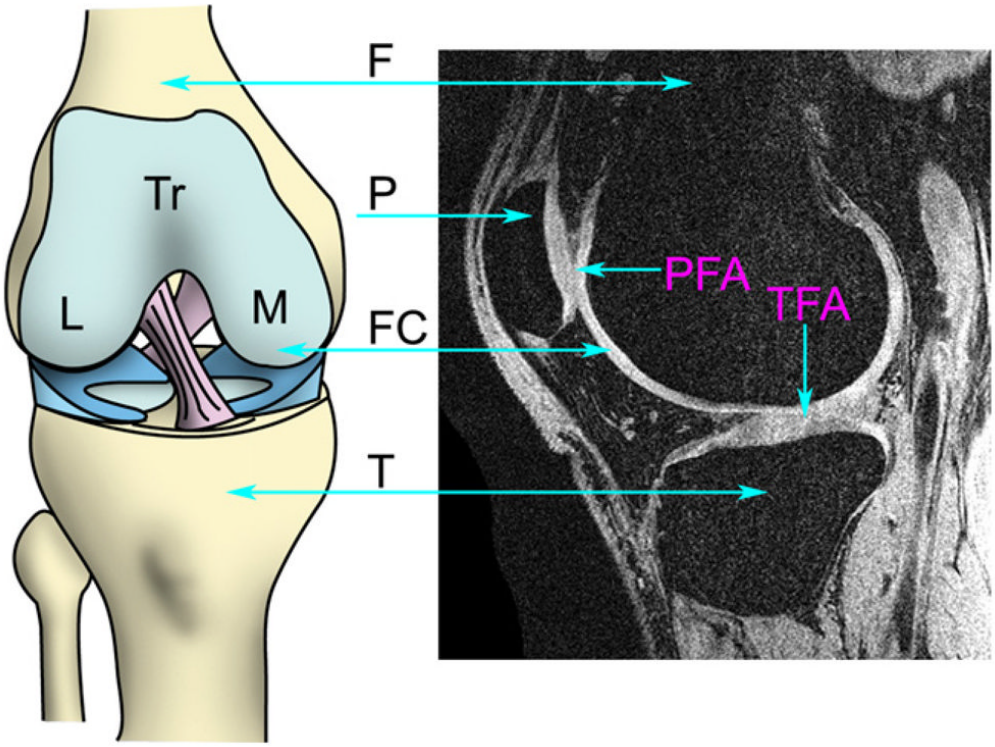

Fig. 1.

Anatomic diagram and sagittal MR image of the knee articulation indicating corresponding structures and compartments. F = Femur; P = patella; T = tibia; FC = femoral cartilage; L = lateral; M = medial; Tr = trochlea; PFA = patello-femoral articulation; TFA = tibio-femoral articulation.

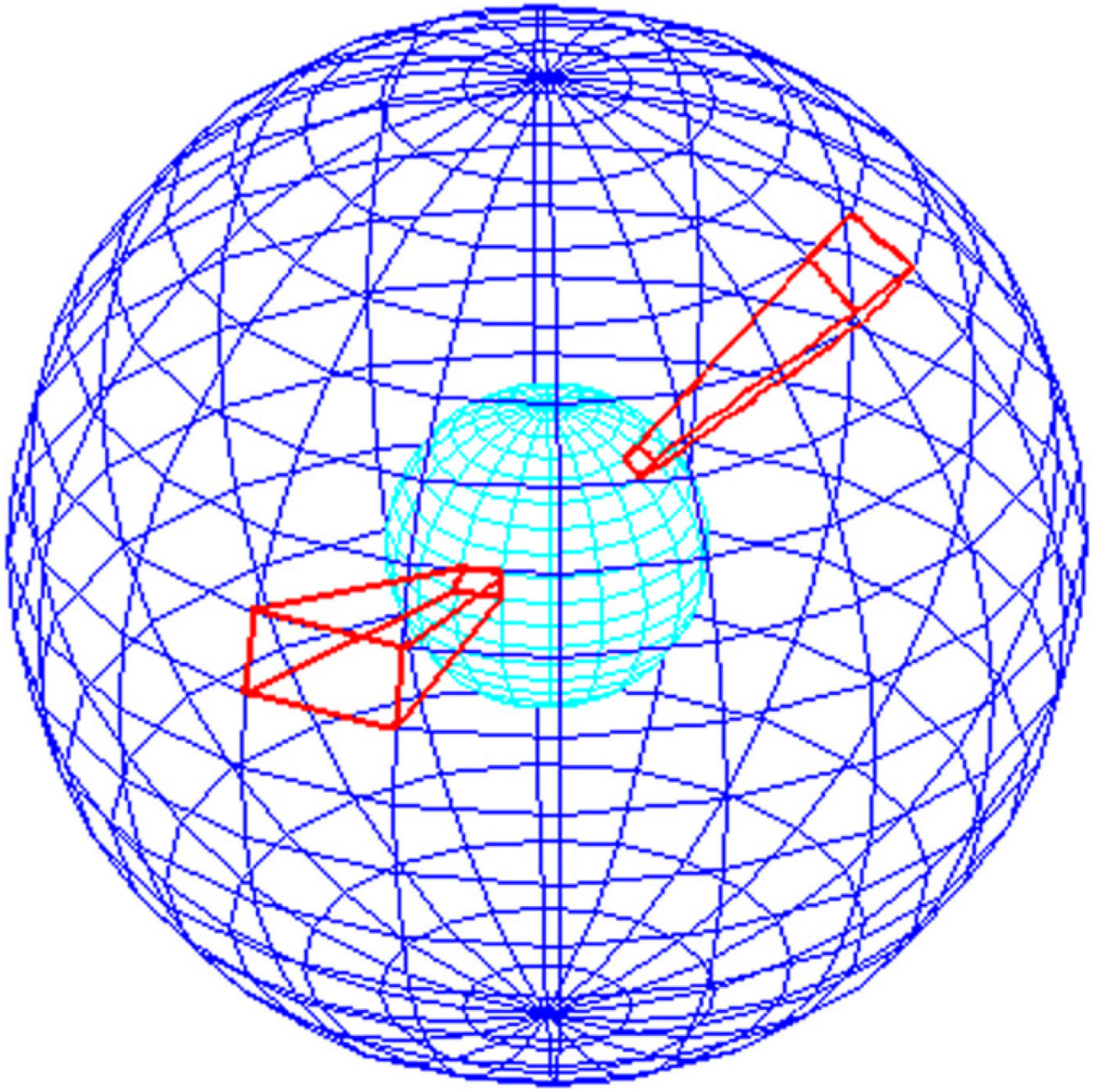

Fig. 2.
Bin distribution of 3D shape context. Radial lines of the log-polar histogram binning structure have been avoided for clarity of representation except for those of the two bins highlighted in red.

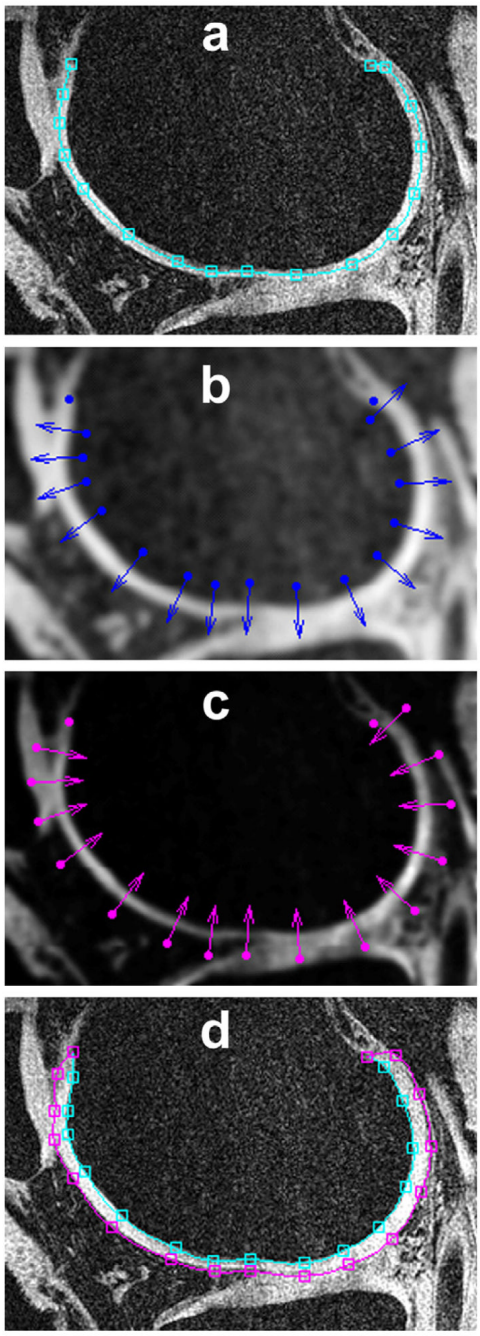

Fig. 3.

Femoral cartilage segmentation of a human knee. (a) Initial Bezier spline defining the shape of the cartilage to be segmented is shown in cyan with its corresponding control points. (b) Blue vectors show the line profiles to find the bone–cartilage interface. (c) Magenta vectors show the line profiles to find the articular surface. (d) Final Bezier splines defining the bone–cartilage interface (cyan) and articular surface (magenta).

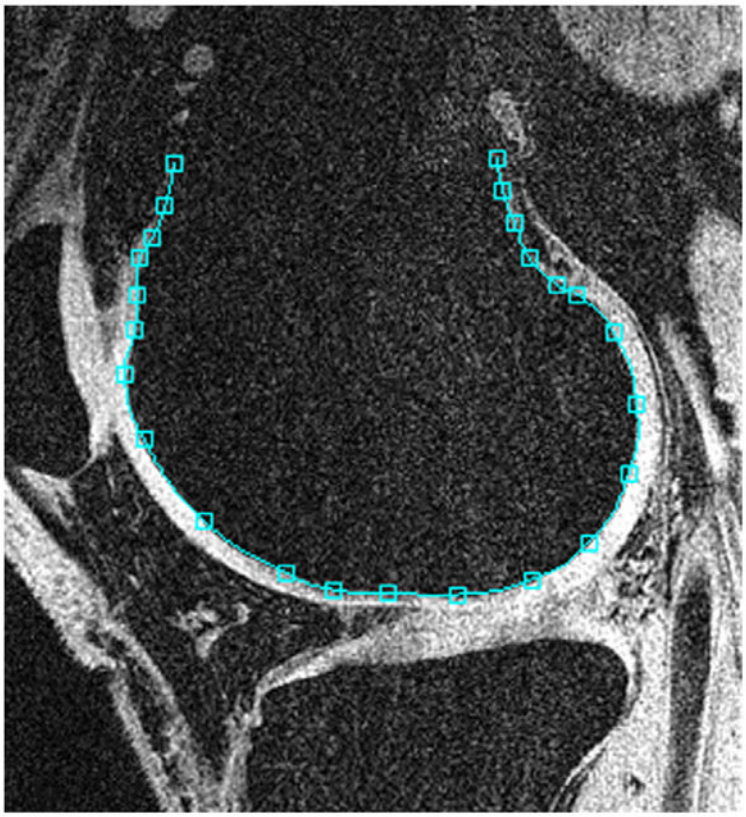

Fig. 4.
Segmentation of the femoral bone using Bezier splines and edge-detection.

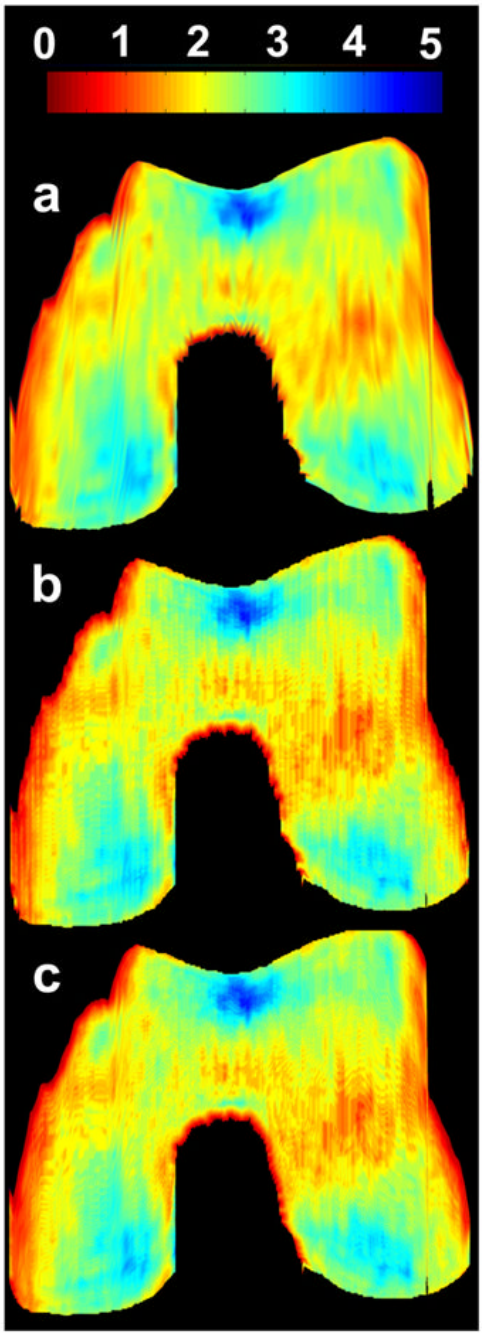

Fig. 5.
Human femoral 3D cartilage thickness maps. (a) Map from non-shape interpolated cartilage. (b) Map from shape-interpolated cartilage based only on DFs. (c) Map from shape-interpolated cartilage based on morphing. Scale bar is in mm.

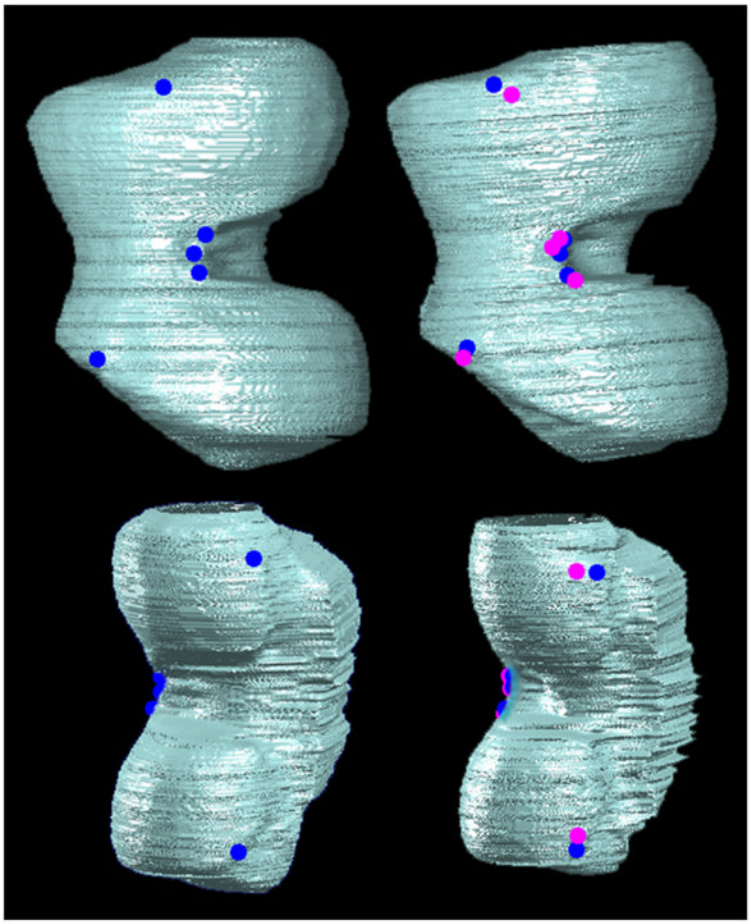

Fig. 6.
Visual representation of inter-subject anatomical point matching. On the left side the target bone is displayed with seven anatomic points selected manually by a radiologist (blue dots), and on the right side the source bone is displayed with the corresponding anatomic points manually selected by a radiologist (blue dots), as well as with the corresponding anatomic points automatically computed (magenta dots) based on those of the target.

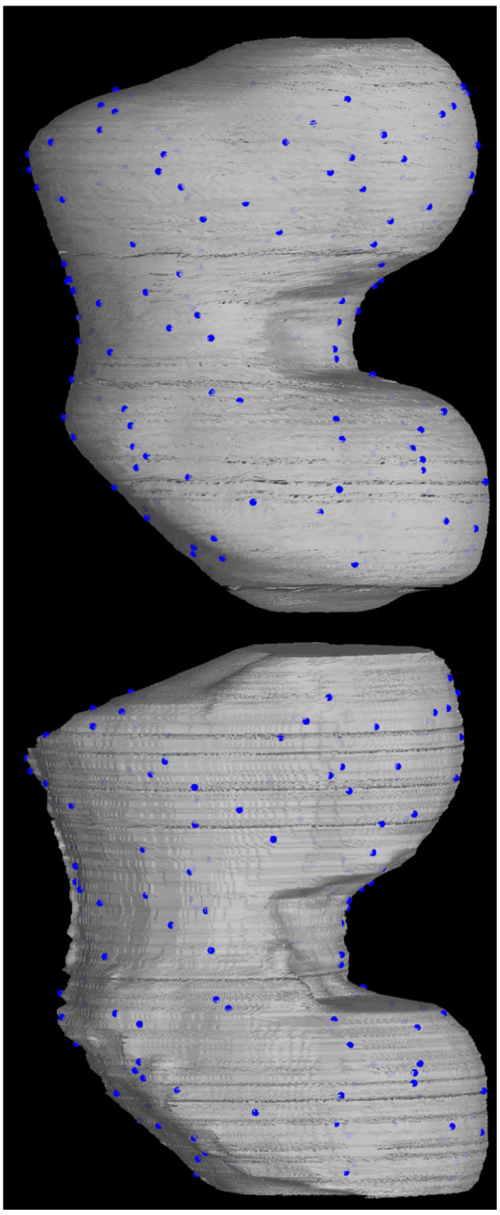

Fig. 7.
Visual representation of automatic point matching. Blue dots represent anatomic points automatically computed for the femoral bone of a subject with severe OA (bottom) based on those automatically and uniformly distributed in the mean femoral shape (top).

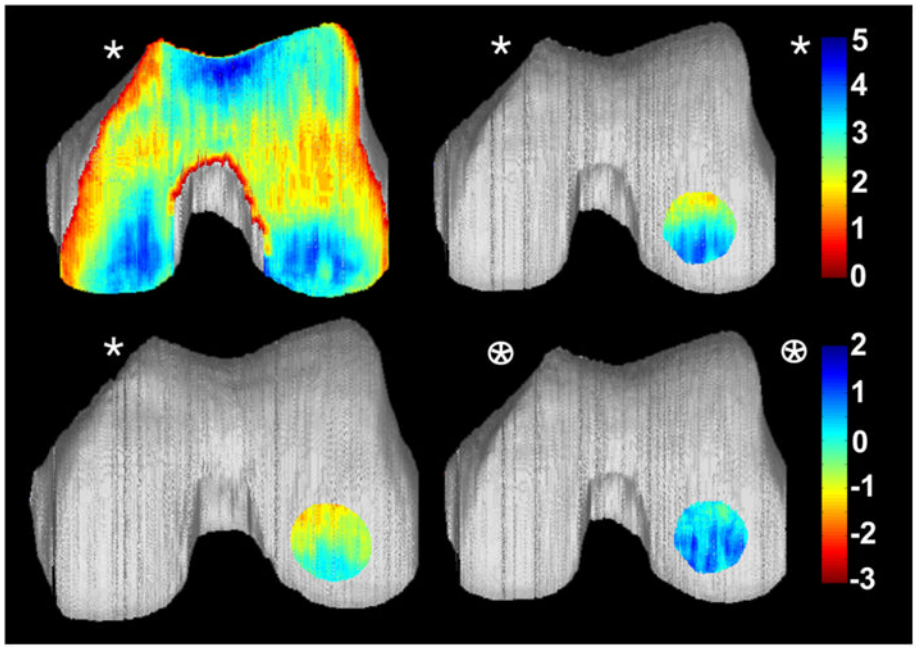

Fig. 8.

Inter-subject cartilage thickness comparison of a small region of interest. *Top row*: Source cartilage thickness map and its matched region. Bottom left: Target cartilage thickness region. *Bottom right*: Source minus target thickness region of interest. Color bars are in mm.

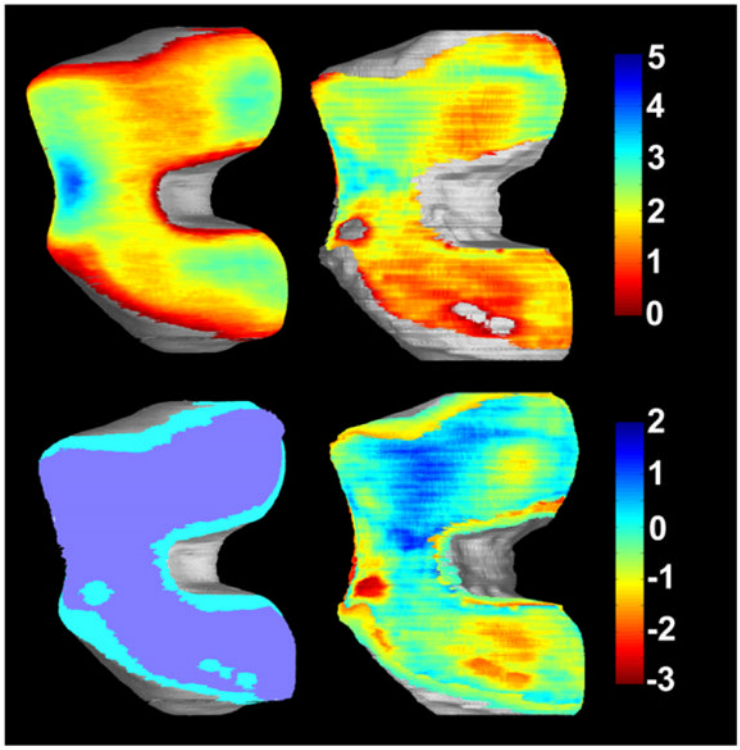

Fig. 9.

Point-wise cartilage thickness comparison using a mean femoral bone shape and cartilage thickness map. *Top left*: Mean femoral cartilage thickness map overlaid on the mean femoral bone shape. *Top right*: Cartilage thickness map of a subject with severe OA overlaid on its femoral bone. *Bottom left*: Overlapping cartilage regions on the mean femoral bone shape after registration. *Bottom right*: Difference thickness map (OA subject minus mean map) overlaid on the bone of the subject with OA. Scale bars are in mm.

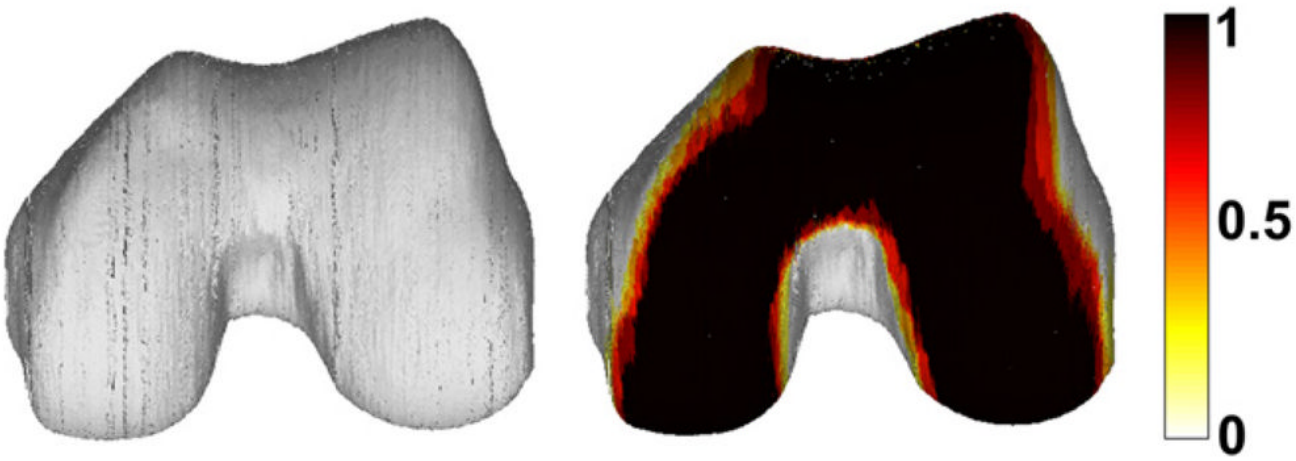

Fig. 10.
Mean femoral bone shape and its corresponding cartilage coverage map. Scale bar represents the probability of the mean bone shape of being covered by cartilage.

Table 1

Reproducibility (CV) of mean intra-subject cartilage thickness measurements with manually delineated baseline and follow-up compartments

Compartment	CV (DFs)	CV (morphing)
All	1.78	1.78
Medial	1.92	2.05
Trochlea	2.26	2.18
Lateral	2.42	2.39

All values are in %. Based on five subjects.

Table 2

Validation results of intra-subject shape matching based on mean distances

	Affine registration based on manually selected target and source anatomic points	**ICP registration based on bone surfaces**	**ICP registration based on bone surfaces → Affine registration based on manually selected target and automatically computed source anatomic points**	**ICP registration based on bone surfaces → Affine registration based on automatically computed target and source anatomic points**
Manually placed target and source anatomic points	2.26	2.65	2.68	2.50
Bone surfaces	0.75	0.77	0.84	0.71
Manually placed target and automatically computed source anatomic points	NA	NA	1.07	NA
Automatically computed target and source anatomic points	NA	NA	NA	1.21

All values are in mm. NA = Not apply. Based on five registrations.

Table 3

Validation results of inter-subject shape matching based on mean distances

	Affine registration based on manually selected target and source anatomic points	**ICP registration based on bone surfaces**	**ICP registration based on bone surfaces → Affine registration based on manually selected target and automatically computed source anatomic points**	**ICP registration based on bone surfaces → Affine registration based on automatically computed target and source anatomic points**
Manually placed target and source anatomic points	3.45	4.98	4.05	4.25
Bone surfaces	1.96	1.95	1.32	1.15
Manually placed target and automatically computed source anatomic points	NA	NA	1.58	NA
Automatically computed target and source anatomic points	NA	NA	NA	1.81

All values are in mm. NA = Not apply. Based on eight registrations.

Table 4

Reproducibility (CV) of localized mean intra-subject cartilage thickness measurements with manually delineated baseline and automatically computed follow-up compartments

Compartment	CV (DFs)
All	2.41
Medial	2.88
Trochlea	2.88
Lateral	2.47

All values are in %. Based on five subjects.

Table 5

Inter-subject comparisons of mean cartilage thicknesses with manually delineated baseline and follow-up compartments

Compartment	CV (DFs)[a]	CV (DFs)[b]
All	10.37	17.32
Medial	8.37	17.75
Trochlea	11.24	16.11
Lateral	14.16	19.25

All values are in %. Based on 10 comparisons.

[a] Target shape is always the baseline scan, e.g. $\text{shape}_{\text{baseline2}} - \text{shape}_{\text{baseline1}}$ vs $\text{shape}_{\text{follow-up2}} - \text{shape}_{\text{baseline1}}$.

[b] Target shape changes, e.g. $\text{shape}_{\text{baseline2}} - \text{shape}_{\text{baseline1}}$ vs $\text{shape}_{\text{follow-up2}} - \text{shape}_{\text{follow-up1}}$.

Table 6

Localized inter-subject comparisons of mean cartilage thickness Differences with manually delineated target and automatically computed source compartments

Compartment	CV (DFs)[a]	CV (DFs)[b]
All	7.50	12.14
Medial	8.58	14.63
Trochlea	12.78	18.82
Lateral	11.16	13.83

All values are in %. Based on 10 comparisons.

[a] Target shape is always the baseline scan, e.g. $\text{shape}_{\text{baseline2}} - \text{shape}_{\text{baseline1}}$ vs $\text{shape}_{\text{follow-up2}} - \text{shape}_{\text{baseline1}}$.

[b] Target shape changes, e.g. $\text{shape}_{\text{baseline2}} - \text{shape}_{\text{baseline1}}$ vs $\text{shape}_{\text{follow-up2}} - \text{shape}_{\text{follow-up1}}$.